

Article

Case Study and Risk Assessment of Water Inrush Disaster in Qingdao Metro Line 4

Yongjun Zhang ¹, Weiguo Zhang ¹, Huangshuai Xia ¹, Bin Gong ^{2,*}, Fei Liu ^{1,3}, Jiahui Zhang ¹ and Kai Liu ¹¹ School of Civil Engineering, Qingdao University of Technology, Qingdao 266520, China² Department of Civil and Environmental Engineering, Brunel University London, London UB8 3PH, UK³ Engineering Research Center of Concrete Technology under Marine Environment, Ministry of Education, Qingdao 266520, China

* Correspondence: bin.gong@brunel.ac.uk

Abstract: Water inrush is one of the most frequent and catastrophic hazards in tunnel engineering, and poses serious threats to the safety of engineering and personnel. This paper presents a case study of a water inrush and ground collapse in the Qingdao Metro Line 4, which caused a cave-in with the diameter and depth of about 30 m and 6 m, respectively. Based on the field data and numerical modelling, the causes of the disaster were analyzed. A numerical model was used to analyze the changes of surface settlement, vault settlement and water pressure during the tunnel excavation. The results of the study indicate that the cause of this disaster was the failure of the tunnel vault surrounding rock caused by the weakening of the tunnel surrounding rock and water pressure, which in turn triggered the water inrush in the tunnel and caused a large volume of surface collapse. As the tunnel was excavated from the slightly weathered area to the strongly weathered area, the vault settlement increased, and the influence zone expanded towards the surface due to the continuous decrease in the strength of the surrounding rock. In particular, a negative pore water pressure zone was formed in a certain area around the tunnel during the water inrush. The negative pressure zone caused the surrounding groundwater to converge here, leading to an increase in the amount of water inflow, which also increased the scope and scale of the impact of this disaster. A risk assessment method for water inrush in tunnels is proposed. According to the geological and engineering characteristics of Qingdao area, the evaluation index system of tunnel water inrush risk was established. An RBF neural network was improved by gray correlation analysis and a PAM clustering algorithm to establish the tunnel water inrush risk assessment model. Comparing the evaluation data with the actual data, the prediction data of a traditional RBF neural network and a BP neural network, the accuracy and reliability of the model were verified. This study has value in reducing the occurrence of water inrush in a composite formation tunnel.

Keywords: water inrush; collapse; numerical model; risk assessmentcheck for
updates

Citation: Zhang, Y.; Zhang, W.; Xia, H.; Gong, B.; Liu, F.; Zhang, J.; Liu, K. Case Study and Risk Assessment of Water Inrush Disaster in Qingdao Metro Line 4. *Appl. Sci.* **2023**, *13*, 3384. <https://doi.org/10.3390/app13063384>

Academic Editor: Arcady Dyskin

Received: 16 February 2023

Revised: 4 March 2023

Accepted: 5 March 2023

Published: 7 March 2023



Copyright: © 2023 by the authors. Licensee MDPI, Basel, Switzerland. This article is an open access article distributed under the terms and conditions of the Creative Commons Attribution (CC BY) license (<https://creativecommons.org/licenses/by/4.0/>).

1. Introduction

As metro construction increases, the pressure of urban surface transportation brought about by urban development and dense population has been greatly alleviated, and metro is the preferred transport mode of people [1,2]. According to statistics from the National Bureau of Statistics, 51 cities in China had opened metro lines by the end of 2021, with a total operating distance of 8736 km. However, water inrush disasters often occur due to geological and groundwater during metro tunnel construction [3]. For example, on 6 May 2011, a water inrush accident occurred during the construction of Tianjin Metro Line 2, and caused the collapse of the road surface. Another example is that on 7 February 2018, in Foshan Metro Line 2, when a water inrush accident occurred and caused the tunnel and roadway to collapse. Water inrush disasters not only cause life and property loss, but also cause environmental problems such as surface collapse and groundwater

loss [4]. Therefore, reducing the occurrence of water inrush is of great significance for safe construction, property loss and environmental protection.

Various methods, such modeling experiments, numerical simulation and field tests have been adopted to explain the mechanism of water inrush. In terms of modeling experiments, various types of models with different sizes and conditions have been proposed to study the process of water inrush. For instance, Li et al. [5] studied the stability of the surrounding rock using a true triaxial geological model test, revealed the internal connections between physical information such as displacement, stress and seepage pressure during tunnel excavation, and established the theoretical basis of the predicting of water inrush. Yang et al. [6] proposed a 3D fluid-solid coupling model test to study the evolution process of water inrush caused by excavation and rainfall, and revealed the mechanism of water inrush. Zhou et al. [7] carried out a seepage instability water inrush test of a karst pipeline to study the evolution process of the filling material seepage instability water inrush and analyzed the changes of surrounding rock displacement, stress, and seepage pressure during the water inrush process. Wang et al. [8] developed a visual experimental system of particle migration to study the mass loss evolution of broken porous rock induced by seepage failure, and discussed the influence of grain gradation on particle migration. However, experimental research is restricted by models without real geological conditions, resulting in difficulty to truly deduce the evolution process of water inrush disaster in engineering. With the development of computers, scholars are addressing this problem using numerical models [9–12]. Li et al. [13] studied the water inrush mechanism in faults of a harbour tunnel by physical and numerical models, and discussed the causality between crown displacement and hydraulic pressure. Jiang et al. [14] revealed the mechanism of water sand inrush in water-rich sandy dolomite strata by a flow-solid coupling model, and analyzed the influence of different factors on the deformation value of the tunnel face. Fan et al. [15] developed a numerical model combining the discontinuous deformation analysis method (DDA) and the smoothed particle hydrodynamics method (SPH) to clarify the water inrush mechanism and the critical thickness of a water-resistant rock mass in a jointed rock tunnel, and divided the process of water inrush into a mutation stage, a cataclysmic stage and a stable stage. Yan et al. [16] studied the mechanism of the collapse of a funnel-shaped stratum through numerical simulation, and found that the essence of the collapse is the process of converting potential energy into kinetic energy. Huang et al. [17] proposed a conceptual model which emphasized the evolution of fracture connectivity to investigate fluid flow through fractured rocks and study the water inrush mechanism, and discussed the influence of the connected fractures on water inflow. Although a numerical model can calculate problems at the engineering scale, results are deficient and ignore the heterogeneity of surrounding rocks. On-site monitoring can reflect the dynamic changes in excavation engineering and the working state of surrounding rock and support [18–20]. Therefore, scholars have also striven to explain the water inrush mechanism based on on-site monitoring data such as surface deformation [21], lining stress [22], water inflow [23,24], and microseismic signals [25]. Previous research has revealed the relationship between disasters and various factors [26–29] that play an important role in reducing the risk during excavation.

Water inrush risk assessment is an important tactic to reduce the occurrence of disaster. The study of tunneling risks started in the 1970s, and Guillermo-Federico [30] first introduced the idea of risk assessment into the field of tunnelling in 1983. Nilsen et al. [31] established a risk assessment structure chart and applied it to a cross-harbour tunnel, based on which Kampmann et al. [32] further improved the risk assessment system and applied it to the metro. Multiple methods have been applied to water inrush risk assessment, including the analytic hierarchy process-AHP [33], cloudy theory [34], Bayesian network [35,36], neural network [37], fuzzy theory [38–40], and other mathematical models. Meanwhile, scholars have continuously improved the original method to obtain more accurate results. For instance, Kim et al. [41] improved the analytic hierarchy process using the Delphi survey technique, and established a probabilistic tunnel collapse risk evaluation model. Aalianvari et al. [42] proposed a risk evaluation model for water inrush combining the

analytic hierarchy process and fuzzy Delphi method, helping to design a more suitable drainage system, drilling method, and support. Wang et al. [43] applied an analytic hierarchy process and fuzzy theory and proposed an interval risk assessment method of water inflow and inrush in karst tunnel. The above-mentioned methods have been effective in reducing engineering risks.

Previous research on the mechanism and risk assessment methods of water inrush have been mostly focused on mountainous and karst areas, while there has been less research on water inrush in the upper soft and lower hard composite strata. Furthermore, for most of the above methods, for the selection of evaluation indexes it has been difficult to eliminate subjectivity. Hence, this study aimed to clarify the water inrush mechanism in composite strata by a case of water inrush and ground collapse in Qingdao Metro Line IV, and proposed a water inrush assessment method based on characteristics of composite strata. First, the case of water inrush and ground collapse is considered. Then, the disaster-causing factors of the water inrush were analyzed comprehensively, and the water inrush mechanism is discussed with respect to a numerical model. Finally, the water inrush risk of the tunnel is evaluated using the improved method. This study has value in reducing the occurrence of water inrush in a composite strata tunnel.

2. Description of the Project and the Collapse

2.1. Project Overview

Qingdao Metro Line IV is the backbone line of the main urban area connecting Shinan District, Shibei District and Laoshan District. The Jing-sha Section is located between Jinggang Road Station and Shazikou Station in Laoshan District, Qingdao City, and its location is shown in Figure 1. After leaving Jinggang Road Station, the section tunnel is laid southward along the middle of Lisha Road, and then deviates from Lisha Road near the intersection of Yugang Road, heading east towards Shazikou Station. The tunnel consists of two parallel single-hole tunnels with a spacing of 13.8 m. The starting and ending mileage of the interval tunnel is (Z) YDK24+739.400–(Z) YDK25+879.000, with a total length of 1139.600 m.

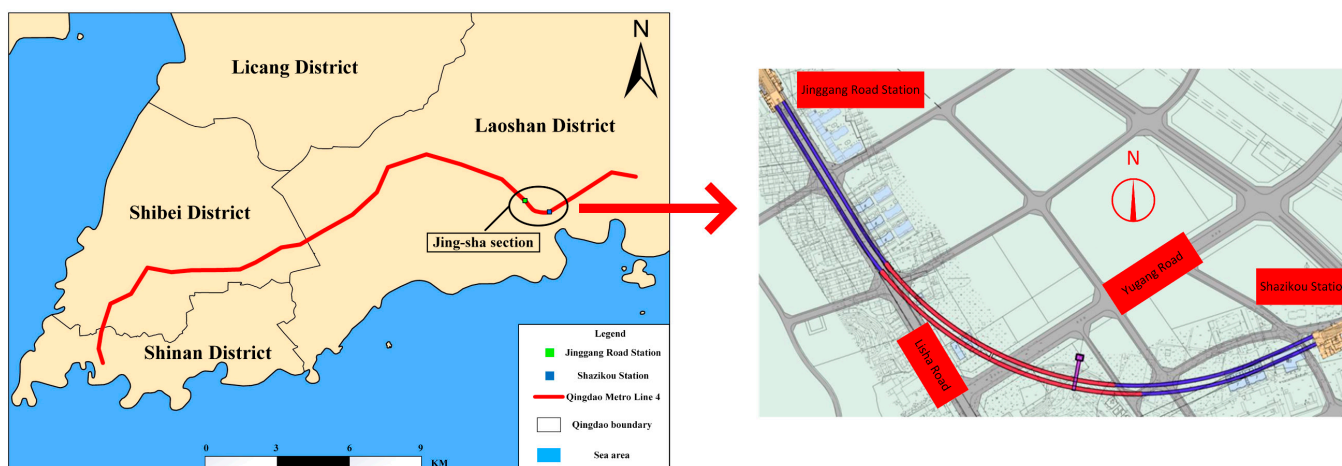


Figure 1. The location of Jing-sha section.

2.2. Geological Conditions

Figure 2 shows the geological profile of the Jing-sha section. The terrain in the section is relatively flat, and the tunnel passes through the corner of Dongjian Mountain at YDK25+355.000~YDK25+504.000. The buried depth of groundwater is 0.8–4.7 m. The stratum is mainly composed of plain fill, silty clay, medium-coarse sand, breccia (moderately weathered granite) and tuff with different weathering degrees. Table 1 shows the physical and mechanical parameters of the different section of ground. The bedrock in the interval is mainly slightly weathered tuff. The buried depth of the section tunnel is about 15.0–33.3 m,

and the thickness of the overburden of the tunnel vault is about 9.5–27.8 m. Silty clay and sand are widely distributed, with the thickness of silty clay and sand being 0.8–4.8 m and 1.2–10.2 m, respectively. The tunnel is mainly located in moderately weathered granite and slightly weathered tuff strata, and partially located in strong and moderately weathered tuff strata.

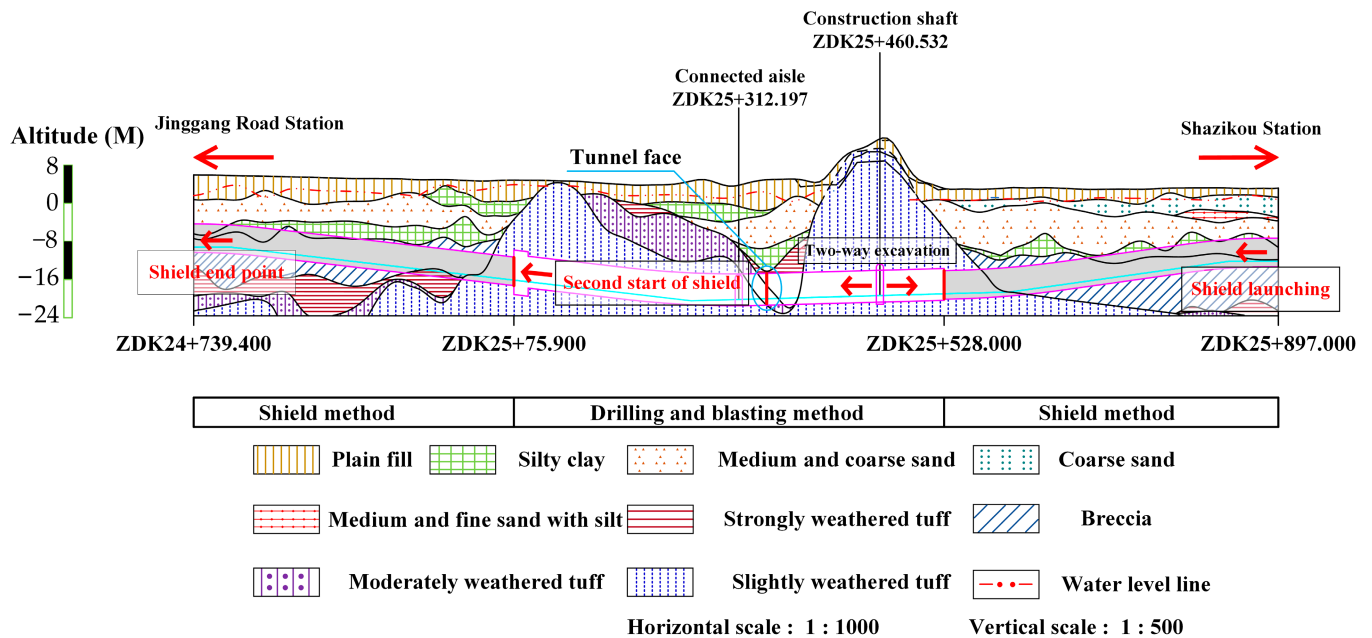


Figure 2. Geological profile of Jing-sha section.

Table 1. The parameters of different ground obtained from the geological report.

	<i>E</i> /kPa	μ	<i>e</i>	<i>K</i> /(m/Day)	<i>C</i> /kPa	φ
Plain fall	8000	0.2	0.9	30	0	15
Silty clay	5671	0.33	0.718	0.05	8.2	12
Sand	6070	0.33	0.5	0.05	13.9	12.5
Strongly weathered tuff	20,000	0.3	0.8	5.1	3.0	30
Moderately weathered tuff	50,000	0.25	0.8	1.728	3000	45
Slightly weathered tuff	5.00×10^6	0.22	0.09	0.026	11,500	55

2.3. Excavation and Support Methods

The construction methods of the tunnel are the shield method and the drilling and blasting method, and the areas used are shown in Table 2. The diameter of the shield tunnel is about 6.3 m. The section and support parameters of the drilling and blasting method tunnel are shown in Figure 3. The tunnel excavation area is about 7.5 m high and 7.4 m wide. The tunnel is excavated by the benching method. It is about 3.7 m high for the upper bench, 3.85 m high for the lower bench, and 3–5 m long for each bench. The initial support of the tunnel is grid steel frame and shotcrete. The grid steel frame spacing is 0.5 m. The shotcrete is C25 concrete with a thickness of about 300 mm. The permanent lining of the tunnel is 300 mm thick molded concrete consisting of C45 waterproof concrete and steel reinforcement. When the tunnel passes through an area with poor surrounding rock properties, $\Phi 42$ advanced small conduits (3.5 m in length and 15° inclination angle) are mounted into the rock in a 120° range around the extrados of the tunnel.

Table 2. Construction method of Jing-sha section.

Interval Mileage	Construction Method	Segment Length
ZDK24+739.400~ZDK25+075.900	shield method	336.500 m
ZDK25+075.900~ZDK25+090.900	The mining method is used as the initial support of the tunnel, and the secondary lining is poured. After the shield enters this section, it is reassembled and debugged, and the second launch is carried out in the mine method tunnel	15.000 m
ZDK25+090.900~ZDK25+528.000	The mine method is used as the initial support of the tunnel, and the second lining is poured after the shield tunnel passes through the	437.100 m
ZDK25+528.000~ZDK25+879.000	shield method	351.000 m
YDK24+739.400~YDK25+063.200	shield method	323.800 m
YDK25+063.200~YDK25+078.200	The mining method is used as the initial support of the tunnel, and the secondary lining is poured. After the shield enters this section, it is reassembled and debugged, and the second launch is carried out in the mine method tunnel	15.000 m
YDK25+078.200~YDK25+568.000	The mine method is used as the initial support of the tunnel, and the second lining is poured after the shield tunnel passes through	489.800 m
YDK25+568.000~YDK25+879.000	shield method	311.000 m

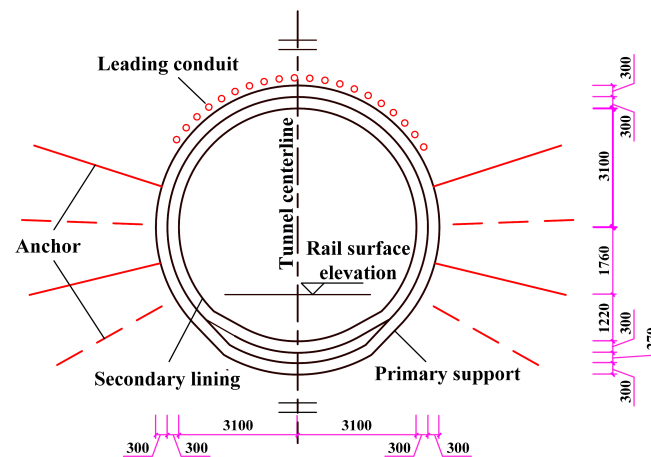


Figure 3. Tunnel section and support parameters (unit: mm).

In addition, due to construction needs, there is a construction shaft and cross passage at YDK25+460.532.

2.4. Details of the Collapse

At about 17:40 p.m. on 27 May 2019, water and mud inrush occurred during the construction of the tunnel in the Jing-sha section, which caused ground collapse. The location of the collapse was ZDK25+343, which is located below Yugang Road, as shown in Figure 4. After the accident, a huge collapse pit with a length of 30 m, a width of 25 m and a height of 6 m was formed on the ground, as shown in Figure 5. It can be seen from the picture that the disaster caused damage to roads, surrounding farmland and underground pipelines. Figure 6 shows the process of collapse. At 15:30 on 27 May 2019, partial water seepage and block falling occurred on the face at ZDK25+343 on the left line, and the face was immediately treated by the conventional treatment method of shotcrete sealing with steel mesh. At about 17:30, closure construction of the face was completed, and there was no water seepage or block falling. At around 17:40, water and mud inrush appeared on the

face. Generally speaking, the disaster developed from partial water seepage on the face of the tunnel, to water and mud inrush, and finally to ground collapse. However, there is no obvious precursor information before the water inrush occurred, which increases the difficulty of disaster identification. After the water and mud inrush occurred, the maximum velocity reached 20.885 m/s, and the mud reached the position of the cross passage (about 110 m from the tunnel face) within 11 s. According to estimates, the volume of sediment in this disaster was about 6924 m³. Figure 7 is a picture of the scene after the tunnel was cleaned up. Traces of muddy water can be clearly seen on the side wall of the tunnel. The height of the muddy water was about 2 m, which shows that the mud once occupied most of the entire tunnel area when the disaster occurred.

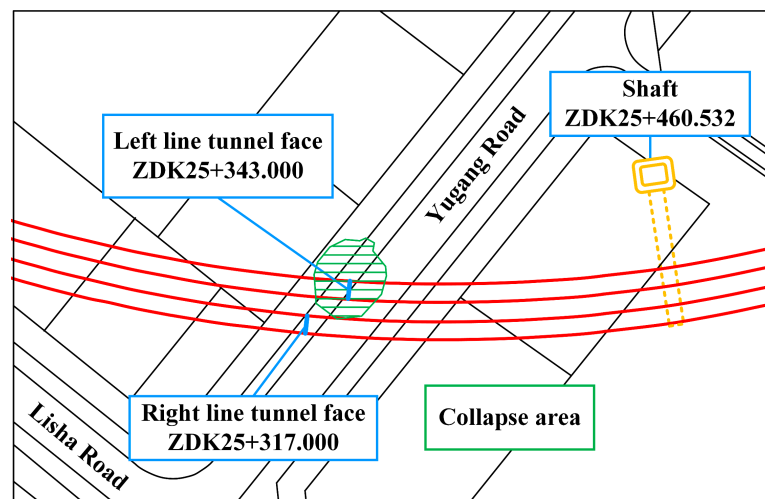


Figure 4. Location of the disaster.

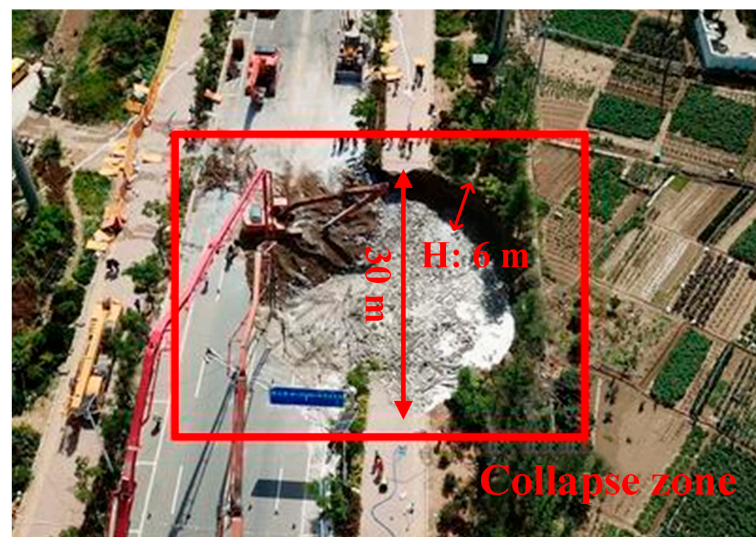


Figure 5. Ground collapse.

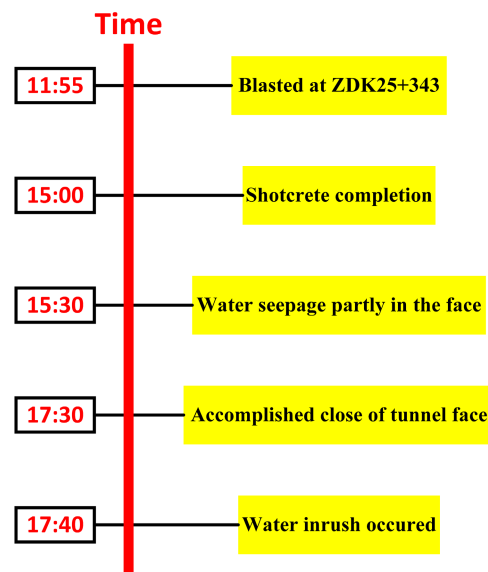


Figure 6. Evolution process of the disaster.



Figure 7. Tunnel after cleaning.

3. Analysis on the Causes of the Collapse

3.1. Factors Leading to the Collapse

It is obvious from Figure 2 that the topography near the disaster location looks like a “funnel”, which made groundwater tend to converge at the bottom of the tunnel. The strata at the disaster location, from top to bottom, consists of a 6.4 m plain fill layer, a 0.8 m silt clay, a 7.1 m medium to coarse sand, a 4.9 m silt clay and tuff with different degrees of weathering. The tunnel is located in strongly weathered tuff and moderately weathered tuff. In the collapse zone, the tunnel passes through the bottom of a “funnel” with a buried depth of approximately 19.6 m, while the water level relative to the top of the tunnel is 19 m. As the tunnel was excavated, groundwater tended to flow into the tunnel at the bottom of the funnel. The strongly weathered tuff at the tunnel vault is extremely fragmented and fissures were developed. Tensile failure and crack expansion of the rock caused by the blasting vibration provided additional water channels. These factors caused the tunnel vault to bear a large water pressure. In this situation, the thickness of strongly weathered tuff at the tunnel vault in the collapsed area is only 0.7 m. According to the statistics, the

cumulative rainfall in the Shazikou area from 11 May to 27 May was 73 mm, as shown in Figure 8. On 17 May, the rainfall was 56.1 mm. From 26–27 May, the rainfall continued for two days with an amount of 4.8 mm. The continuous rainfall provided ample recharge of groundwater, which worsened the situation. These two main factors are further analyzed in the next section.

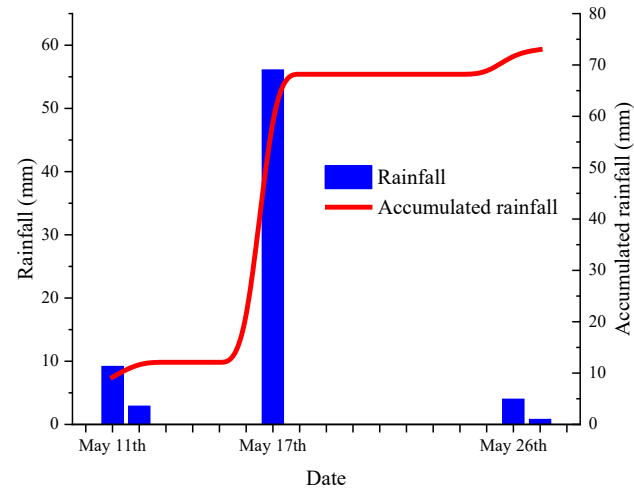


Figure 8. Rainfall in Shazikou area.

3.2. Numerical Simulation for the Collapse

3.2.1. Establishment of Numerical Models

In this section, a numerical model is described to study the evolution of the disaster. Based on the practical geological of the tunnel from ZSK 25+270 to ZSK 25+395, a three-dimensional finite element numerical model was established by Midas GTX NX, as shown in Figure 9. The model size was $75\text{ m} \times 125\text{ m} \times 50\text{ m}$, and the buried depth of tunnel was 19.6 m. In the numerical model, the yield condition, and the Mohr-Coulomb model, was used. The parameters of the model were taken according to Table 1. In accordance with the actual construction method of the project, the tunnel was excavated using the benching method. The left tunnel face was ahead of the right tunnel face with an interval of 10 m, with a single bench length of 5 m. The tunnel excavation range was from ZDK25+340 to ZDK25+395. After the excavation of each bench, C25 concrete with a thickness of 300 mm was used as the initial support, and the parameters are shown in Table 3. The groundwater level was set at -1 m . The left, right and bottom of the model are impermeable boundaries, and the surface of tunnel excavated was set as the permeable boundary.

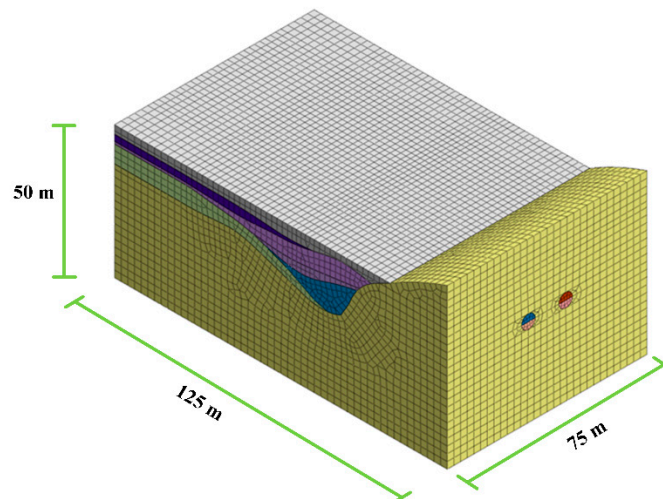


Figure 9. Numerical model of tunnel.

Table 3. The empirical parameters of concrete.

	<i>E</i> /kPa	μ	<i>e</i>	<i>K</i> /(m/Day)	<i>C</i> /kPa	φ
Plain fall	8000	0.2	0.9	30	0	15
Silty clay	5671	0.33	0.718	0.05	8.2	12
Sand	6070	0.33	0.5	0.05	13.9	12.5
Strongly weathered tuff	20,000	0.3	0.8	5.1	3.0	30
Moderately weathered tuff	50,000	0.25	0.8	1.728	3000	45
Slightly weathered tuff	5.00×10^6	0.22	0.09	0.026	11,500	55
C ₂₅ concrete	2.20×10^7	0.2	0.01	8.64×10^{-5}	20,000	60

3.2.2. Analysis of Settlement Results

Figure 10 shows the settlement of the ground during excavation. The slightly weathered tuff is the dominant lithology from ZDK25+395 to ZDK25+360, and the grade of surrounding rock is III. Figure 10a,b shows the settlement of the tunnel during the excavation from ZDK25+395 to ZDK25+360. It can be seen from these pictures that the influence zone on the surrounding rock caused by excavation is minor, while the ground surface is basically unaffected. During this period, the excavation caused minor vault settlement, with a maximum settlement value of -0.16 mm. The strongly weathered tuff is the dominant lithology from ZDK25+360 to ZDK25+340, and the grade of surrounding rock is V. When excavated to ZDK25+355, the tunnel is located at the junction of slightly weathered tuff and strongly weathered tuff. During the excavation here, the tunnel vault in the strongly weathered tuff area settled significantly with a settlement value of -7.77 mm, as shown in Figure 10c. Meanwhile, the influence zone of the tunnel excavation started to extend towards the surface. When excavated to ZDK25+350, the surrounding rock of the tunnel consisted entirely of strongly weathered tuff. At this point, tunnel excavation caused significant settlement and had a large impact. Surface settlement was the largest factor, with a settlement value of -31.82 mm, as shown in Figure 10d, which exceeded the warning value of 30 mm required for tunnel monitoring. When excavated to ZDK25+340, the collapse zone, the surface settlement value increased to 52.47 mm, as shown in Figure 10e.

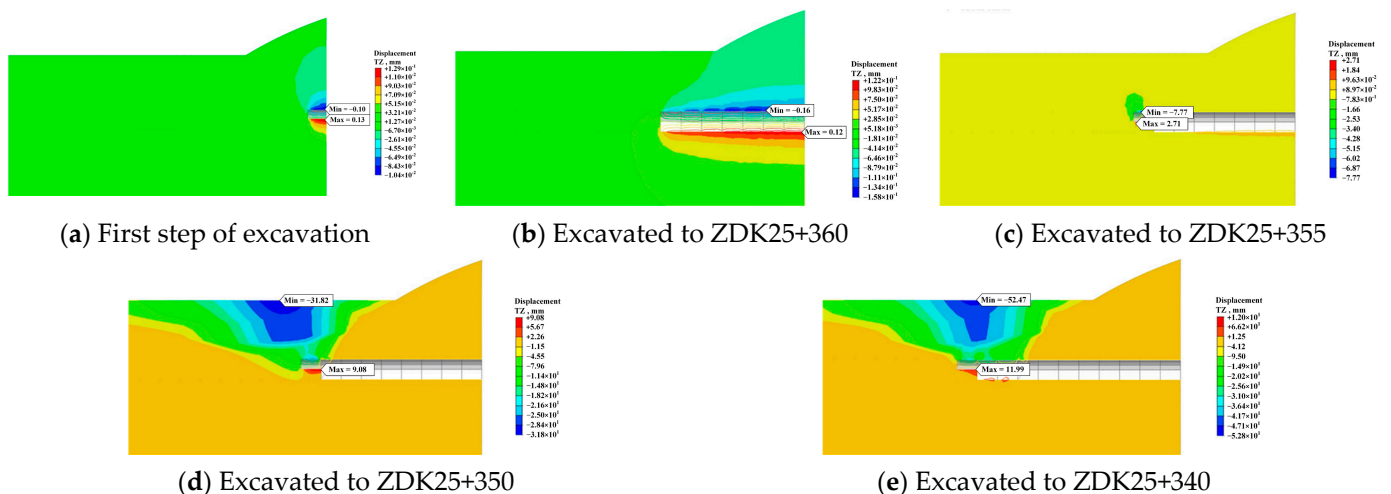


Figure 10. Settlement of the ground.

After excavation, near ZDK25+343, a cave-in with the diameter of 30 m appeared in the model, as shown in Figure 11. The actual collapse location is ZDK25+343, and the diameter of the collapse pit is about 30 m. The simulation results are consistent with the actual situation, indicating that the simulation is reliable.

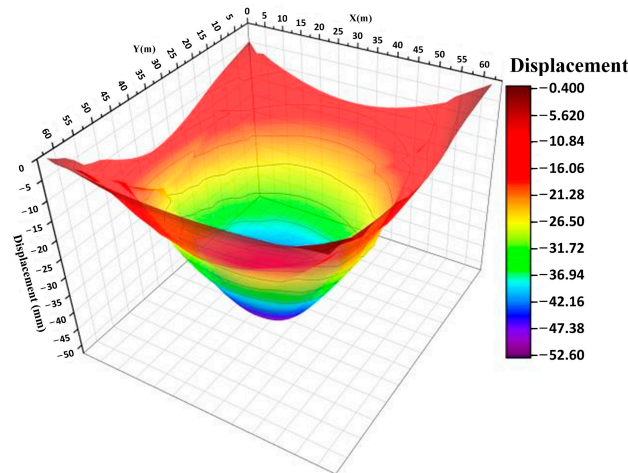


Figure 11. Cave-in zone in model.

Before excavation, many monitoring points were set up at the surface. The distribution of monitoring points near the disaster area is shown in Figure 12. As can be seen from the figure, there are three groups of monitoring points located in the collapse area, namely ZDBC67, ZDBC68 and ZDBC69. The surface settlement of these three groups of monitoring points 7 days before the collapse is shown in Figure 13. From the figure, it can be seen that the collapsed area had a large settlement before the accident, and the maximum value of surface settlement was about 30 mm at ZDBC69-1. In particular, ZDBC67-2 showed a significant settlement abruptness with a deformation rate of 4.50 mm/d on 23 May. Corresponding to the locations of the three groups of monitoring points, the surface deformation data of the model during the excavation from ZDK25+355 to the collapse zone were extracted, and the results are shown in Figure 14. It can be seen from the figure that when excavated to ZSK25+355, i.e., at the intersection of strongly weathered tuff and slightly weathered tuff, the surface settlement was already large, and the maximum surface settlement was about 28 mm at ZDBC69-1. As the tunnel was excavated, ground deformation gradually increased. When excavated to the collapse zone, the maximum value of surface deformation was about 30 mm, which reached the warning value.

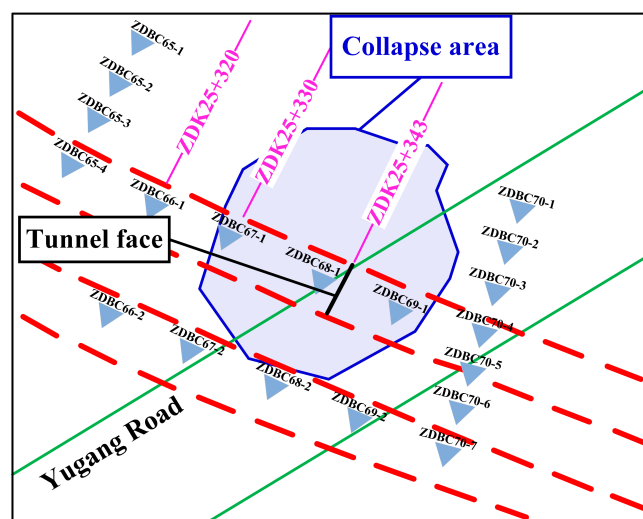


Figure 12. Distribution of monitoring points.

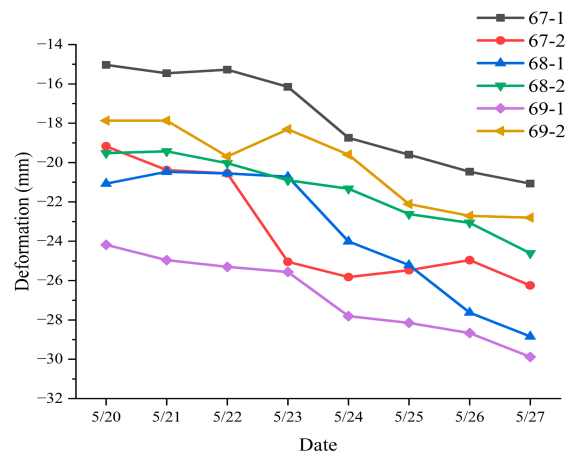


Figure 13. Surface settlement.

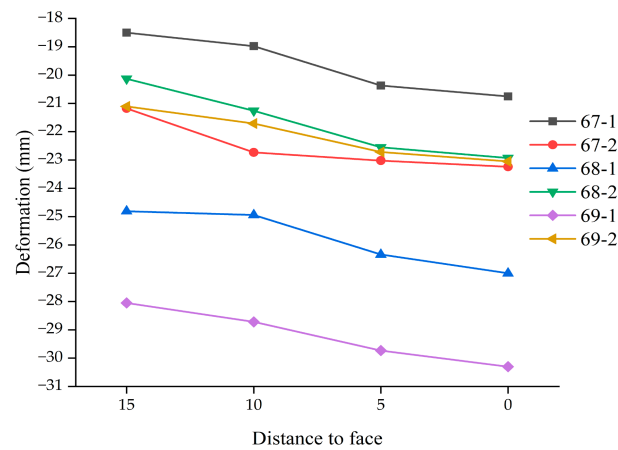


Figure 14. Surface deformation at monitoring points.

Figure 15 shows the deformation of the tunnel vault surrounding rock in the collapse zone during the simulation. Due to construction disturbance, the stratum in the collapse zone had settled before construction. When the excavation reached ZDK25+355, the tunnel vault settled obviously with a value of about 5 mm. When the excavation reached ZDK25+343, the settlement caused by the excavation increased abruptly, with a settlement value of 28.57 mm. The cumulative settlement during excavation reached 37.44 mm, which exceeded the warning value.

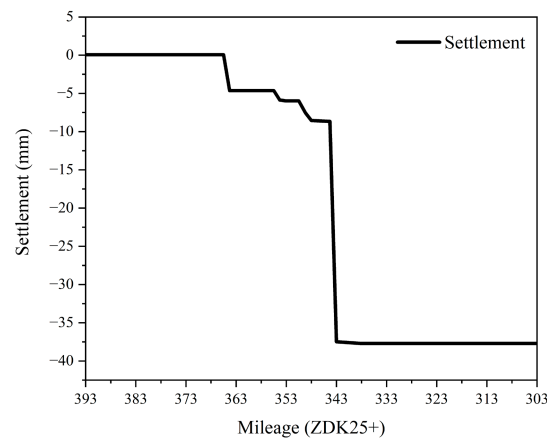


Figure 15. Settlement of the tunnel vault.

Comprehensive analysis of the monitoring data and simulation data showed that when the tunnel was excavated to the strongly weathered area, especially at the bottom of the funnel, the surface settlement as well as the vault settlement changed significantly, which indicated that adverse geological factors led to the disaster.

3.2.3. Analysis of Seepage Results

After tunnel excavation, the groundwater seeped towards the tunnel, as shown in Figure 16. As can be seen from the figure, when groundwater converged toward the bottom of the funnel, most of the groundwater bypassed the powdered clay layer due to the poor permeability of the powdered clay, which plays a certain role in water isolation. In this circumstance, the groundwater is more likely to seep downward from above the tunnel vault, resulting in a greater possibility of seepage failure of the surrounding rock.

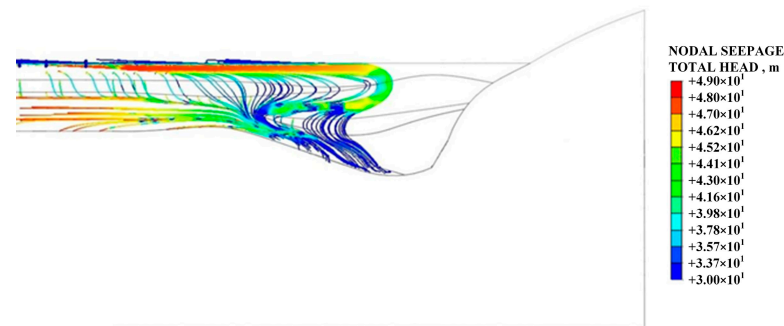


Figure 16. Groundwater seepage.

Figure 17 shows the pore water pressure of the ground at the time of the disaster. It can be seen from the figure that a negative pore water pressure zone was formed in a certain area around the tunnel when the disaster occurred. This indicates that the rate of groundwater loss in the region was greater than the rate of recharge. The existence of a negative pressure area increased the groundwater recharge, which indicates that water inrush would cause a larger range of groundwater recharge to the zone and result in an amount of water inflow far beyond the normal amount of water inflow in the area. This, water inrush caused a large amount of groundwater to gush into the tunnel and cause damage to the upper soil layer, causing the ground to collapse. At the site, the volume of water was about 4755.8 m³. According to the empirical formula of maximum water inflow in the Railway Code, as shown in Equation (1), the maximum water inflow in the area would be 4154.4 m³, which is less than the actual value.

$$Q = 0.0255 + 1.9224KH \quad (1)$$

where K is the permeability coefficient of aquifers, and H is the distance from the resting water level to the center of the equivalent circle of the cave cross-section. Inadequate estimation of the water inflow in the tunnel was an important cause of the accident. The water inrush caused the groundwater level to drop significantly, causing the soil to consolidate and create ground subsidence.

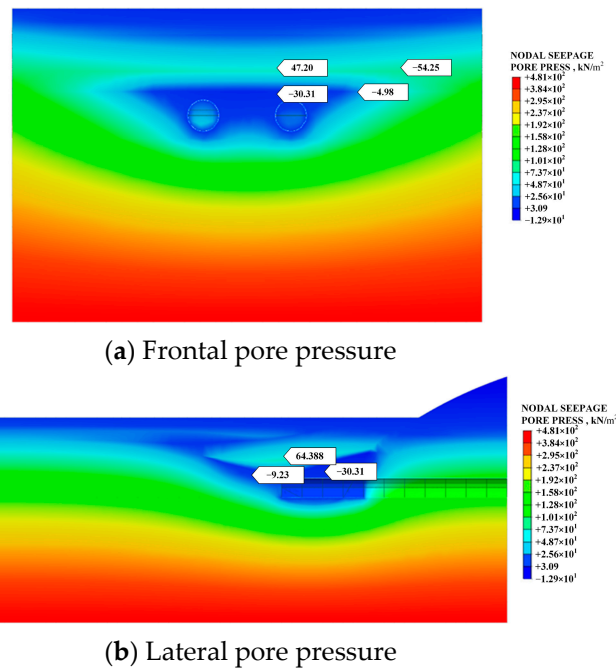


Figure 17. Negative pressure zone.

4. Water Inrush Risk Assessment

4.1. Evaluation Index System for Water Inrush Risk

The main risk factors inducing water inrush disasters in tunnels include geological structure, landform, tunnel and surrounding rock conditions, and hydrological conditions [44]. Based on the geological characteristics of the Qingdao area, which is soft at the top and hard at the bottom, and combined with the actual engineering problems encountered in the excavation process of the Qingdao subway, the water inrush risk evaluation index system for subway tunnels in Qingdao area was established, as shown in Table 4.

Table 4. Risk assessment index system for tunnel water inrush in the Qingdao area.

Level 1 Indicators	Secondary Indicators	Levels of Danger			
		C ₄ (Low Risk)	C ₃ (Medium Risk)	C ₂ (High Risk)	C ₁ (Very High Risk)
Tunnel and surrounding rock conditions I ₁	Tunnel excavation width I ₁₁	<8.5	[8.5, 12)	[12, 14)	≥14
	Tunnel depth I ₁₂	<10	[10, 30)	[30, 50)	≥50
	Rock integrity I ₁₃	whole	broken	Broken	extremely broken
	Rock saturated uniaxial compressive strength I ₁₄	>60	(30, 60]	(15, 30]	≤15
	Degree of crack expansion I ₁₅	underdeveloped	development	more developed	very developed
	Basic quality grade of rock mass I ₁₆	I, II	III	IV	V
Geological structure and surface factors I ₂	Fault fracture zone width I ₂₁	<50	[50, 100)	[100, 300)	≥300
	Catchment area/%I ₂₂	<20	[20, 40)	[40, 60)	≥60
	Topography I ₂₃	flat	slope	steep terraces, valleys	denuded mounds, eroded plains
	Composite ratio of soft and hard formations/%I ₂₄	<25	[25, 50)	[50, 75)	≥75
Hydrological conditions I ₃	Water richness of groundwater I ₃₁	no water	slightly watery	watery	rich in water
	Elevation difference of groundwater I ₃₂	<10	[10, 30)	[30, 60)	≥60
	Permeability coefficient I ₃₃	<0.01	[0.01, 1)	[1, 10)	≥10
	Average monthly rainfall I ₃₄	<60	[60, 80)	[80, 100)	≥100

4.2. A Novel Risk Assessment Method

An RBF neural network is a typical single hidden layer feedforward neural network, including an input layer, a hidden layer and an output layer. By mapping, the RBF neural network can transform low-dimensional, inseparable, original data into high-dimensional, linearly separable data, and obtain the implicit law of the original data to perform training fitting and evaluation prediction. At present, RBF neural networks are widely used in the fields of medicine, economy, and the environment. However, they are rarely used in tunnel water inrush risk assessment. The RBF neural network uses radial basis functions, a real-valued function that takes values that depend only on the distance from the centroid, as a mapping relationship to form the input layer data into the hidden layer space. Therefore, the choice of the center point of the RBF neural network is crucial to the performance of its network. Based on this, a PAM clustering algorithm was used to determine the center c of the hidden layer and the expansion constant σ_i to improve the accuracy of the RBF neural network. On the other hand, when using a neural network for learning, the more raw the data, the longer the calculation time and the larger the dimension. In actual computing, dimensionality reduction is often performed on the original data to reduce computing time. In the process of tunnel water inrush risk assessment, conventional dimensionality reduction methods invalidate the physical meaning and research significance of the data itself, which leads to the invalidation of the data. To ensure that the initial information is not corrupted, gray correlation analysis is introduced to reduce the dimensionality of the data.

Through the combination of gray relational analysis, a PAM clustering algorithm and RBF neural network, a tunnel water inrush risk assessment model was established. The evaluation process of the model is shown in Figure 18.

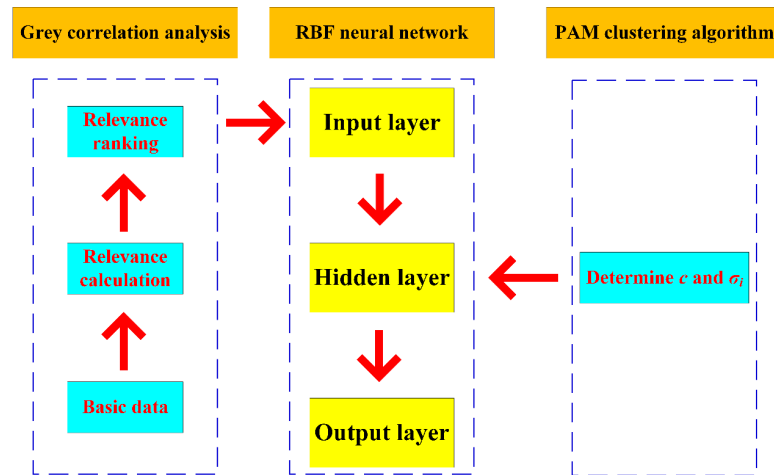


Figure 18. Improved RBF neural network.

4.3. Application of Proposed Model

4.3.1. Training of Improved RBF Neural Network

According to the water inrush risk evaluation index system proposed in Section 4.1, the relevant indicators of the Kaisheng section of Qingdao Metro Line 1, the Wunan section of Qingdao Metro Line 2, and the Shimiao section of Qingdao Metro Line 2 were selected, as shown in the Table 5. These were used as the training data of the RBF neural network.

Table 5. Training sample data.

Tunnel Name	Sample	Grade	I ₁₁ /m	I ₁₂ /m	I ₁₃	I ₁₄ /MPa	I ₁₅	I ₁₆	I ₂₁ /%	I ₂₂	I ₂₃ /%	I ₃₁	I ₃₂ /m	I ₃₃ /md ⁻¹	I ₃₄ /mm
Kaisheng Section of Qingdao Metro Line 1	1	I	6.2	12.6	whole	44.23	underdeveloped	II	41.35	flat	39.68	slightly watery	3.01	0.0043	59.5
	2	II	6.2	12.8	broken	44.23	more developed	IV	69	flat	84.4	rich in water	8.84	2.8512	59.5
	3	IV	6.2	14	extremely broken	11.97	development	V	77.21	flat	85.7	rich in water	12	4.4928	59.5
	4	IV	6.2	13.95	extremely broken	10.8	very developed	VI	75	slope	91	rich in water	10.47	25.92	59.5
Wunan section of Qingdao Metro Line 2	5	II	5.2	11.6	broken	137.3	more developed	IV	11	slope	34.48	slightly watery	1.28	0.0013	57.9
	6	IV	5.2	11.5	extremely broken	28.2	very developed	V	28.43	slope	69.56	watery	3.27	5.184	57.9
	7	II	5.2	11	broken	28.2	very developed	V	0.1	flat	21.8	no water	0.1	0.0042	57.9
	8	II	5.2	10.4	broken	137.3	more developed	V	31.25	flat	53.84	slightly watery	3.25	5.184	57.9
Shimiao section of Qingdao Metro Line 2	9	IV	6.4	13.6	broken	15.6	development	VI	77.43	slope	94.12	rich in water	9.73	15	57.9
	10	III	6.4	16	broken	26	more developed	V	74.5	flat	93.75	rich in water	11.92	0.1	57.9
	11	I	6.4	9.8	whole	57.3	underdeveloped	IV	1.63	denuation mound	92.65	slightly watery	0.16	0.01	57.9
	12	IV	6.4	15.6	extremely broken	6.5	very developed	VI	84.1	flat	91.76	rich in water	13.12	0.5	57.9

The training data were dimensionally reduced by grey correlation analysis. Taking the risk level as the parent sequence and the quantitative index value as the subsequence, we calculated the gray correlation coefficient between the subsequence and the indicators of the parent sequence and averaged them to obtain the correlation degree of each indicator, as shown in Table 6. Before calculation, all data were nondimensionalized using the initial value method to reduce analytical errors.

Table 6. Index correlation.

Quantitative Index Value	I ₁₁	I ₁₂	I ₁₃	I ₁₄	I ₁₅	I ₁₆	I ₂₁	I ₂₂	I ₂₃	I ₃₁	I ₃₂	I ₃₃	I ₃₄
Correlation	0.848	0.862	0.925	0.675	0.923	0.878	0.831	0.825	0.900	0.892	0.817	0.718	0.832

The indicators were sorted according to their correlation degree, and the first 12 index values with high correlation degree were selected as input values. The 12 sets of sample data were input as training data, and the actual water inrush risk levels (low risk, medium risk, high risk, and very high risk) were represented by numbers 1, 2, 3, and 4. In order to ensure the accuracy of the model, the optimal number of clusters was set to k = 4, and the maximum number of iterations when selecting the center for PAM clustering was 600 times. The improved RBF neural network was trained by the gradient descent method, the err-goal was 0.005, and the maximum number of iterations was set to 10,000. The training prediction results were completely consistent with the training samples, as shown in Table 7, indicating that the model met the training requirements.

Table 7. Comparison table of prediction results and training samples.

Sample	Risk Level												
Test-out	1	2	4	4	2	4	2	2	4	3	1	4	
Sam-out	I	II	IV	IV	II	IV	II	II	IV	III	I	IV	

Three parameters of different mileage in the static sediment interval were selected as the test sample data. According to the geological survey report and construction site data, the risk index parameters of water inrush in the static sand section were obtained through sorting, as shown in Table 8.

Table 8. Risk index data of water inrush in each tunnel section of Jingsha section of Qingdao Metro Line 4.

Sample	Risk Level	I ₁₁ /m	I ₁₂ /m	I ₁₃	I ₁₄ /MPa	I ₁₅	I ₁₆	I ₂₁ /%	I ₂₂	I ₂₃ /%	I ₃₁	I ₃₂ /m	I ₃₃ /md ⁻¹	I ₃₄ /mm
1	I	7.4	16.2	whole	93.22	underdeveloped	II	21.6	flat	16.2	watery	1.4	0.0026	118.6
2	III	7.4	17.74	broken	45.3	development	IV	77.2	flat	87.4	rich in water	15.94	0.5184	118.6
3	IV	7.4	16.6	broken	45.3	development	VI	95.6	flat	98	rich in water	15.88	0.5184	118.6

Note: sample 1: ZDK2+111.120~ZDK25+137.800; sample 2: ZDK25+137.800~ZDK25+296.800; sample 3: ZDK25+528.000~ZDK25+879.000.

Three groups of test samples were evaluated for water inrush risk level, and the same data, which had been processed, was used to evaluate water inrush risk level through a traditional RBF neural network and BP neural network. The evaluation results are shown in Table 9.

Table 9. Gray relational PAM improved RBF neural network tunnel water inrush risk assessment results.

Sample	Risk Level	Model Prediction		
		Gray Relational PAM Improves RBF	RBF	BP
1	I	I	I	I
2	III	III	IV	III
3	IV	IV	IV	III
mean square error		0.0461	0.2500	0.7787

It can be seen from Table 8 that the risk level of water inrush in the Jing-sha section of Qingdao Metro Line 4 predicted by the model was completely consistent with the actual risk level, indicating that the results of the model were reliable. In addition, compared with the traditional RBF neural network model and the BP neural network model, this model had higher prediction accuracy, better performance, smaller mean square error and did not easily fall into the local optimal solution, indicating that the improved RBF neural network model could better fit the complex relationship between the risk level of water inrush and various factors.

4.3.2. Water Inrush Risk Assessment of Jing-Sha Section

Using the proposed model, the risk assessment of water inrush was carried out for the tunnel in the section from ZDK25+296.800 to ZDK25+402.130. The parameters of water inrush risk indicators in this interval are shown in Table 10.

Table 10. Parameters of water inrush risk indicators in the Jing-sha interval ZDK25+296.800~ZDK25+402.130.

I ₁₁ /m	I ₁₂ /m	I ₁₃	I ₁₄ /MPa	I ₁₅	I ₁₆	I ₂₁ /%	I ₂₂	I ₂₃ /%	I ₃₁	I ₃₂ /m	I ₃₃ /md ⁻¹	I ₃₄ /mm
7.4	16.2	whole	93.22	underdeveloped	II	21.6	flat	16.2	slightly watery	1.4	0.0026	118.6
7.4	17.74	broken	45.3	development	IV	77.2	flat	87.4	rich in water	15.94	0.5184	118.6
7.4	16.6	broken	45.3	development	VI	95.6	flat	98	rich in water	15.88	0.5184	118.6

Through calculation, the risk level of water inrush in this zone was IV, for special high risk. In fact, the water inrush accident introduced in 2.4 occurred in this interval, which is consistent with the predicted results. Through the risk level evaluation and identification of water inrush risk areas, staff could carry out safety protection procedures in advance, thereby reducing the occurrence of water inrush accidents during the construction process.

5. Conclusions

To investigate the disaster and clarify the causes of the disaster, a field survey and numerical simulation were conducted. A risk assessment method for tunnel water inrush was proposed to evaluate the risk. The main conclusions are as follows:

A funnel-shaped formation makes the groundwater converge towards the tunnel. The thickness of strongly weathered tuff at the tunnel vault in the collapsed area is only 0.7 m. At the same time, heavy rainfall increased the groundwater level and the water pressure. These geological conditions became the trigger factors of the accident.

This disaster was significant because of the poor surrounding rock and seepage pressure. When the tunnel was excavated from the slightly weathered area to the strongly weathered area, deformation increased abruptly. As the excavation proceeded, the excavation-affected area gradually expanded to the surface. The monitoring and simulation data showed that when the tunnel was excavated in the strongly weathered area, the surface settlement approached the warning value quickly. In addition, after the disaster, a negative pore water pressure zone formed around the tunnel, and increased the scope and scale of the accident as the water converged here.

A risk assessment index system for tunnel water inrush in Qingdao area is proposed. An improved RBF neural network was established by combining gray correlation analysis and a PAM clustering algorithm, and its reliability was verified. The water inrush risk level of the Jing-sha section was very high risk at level IV, which corresponds to the actual situation (water inrush). Making a proper risk assessment and taking the corresponding measures can effectively reduce engineering risks.

Author Contributions: Conceptualization, Y.Z. and B.G.; methodology, Y.Z. and B.G.; investigation, Y.Z., W.Z. and H.X.; formal analysis, H.X. and F.L.; validation, J.Z. and K.L.; data curation, Y.Z.; funding acquisition, Y.Z.; supervision, Y.Z. and B.G.; writing—original draft, Y.Z., W.Z. and H.X.; writing—review and editing, B.G. All authors have read and agreed to the published version of the manuscript.

Funding: This research was funded by the Demonstration Project of Benefiting People with Science and Technology of Qingdao, China (Grant No. 23-2-8-cspz-14-nsh), the Shandong Provincial Natural Science Foundation, China (Grant No. ZR2022QD102) and the National Natural Science Foundation of China, China (Grant No. 51674151).

Institutional Review Board Statement: Not applicable.

Informed Consent Statement: Not applicable.

Data Availability Statement: The datasets generated and/or analyzed during the current study are available from the corresponding author upon reasonable request.

Conflicts of Interest: The authors declare no conflict of interest.

References

1. Xie, H.; Leung, C.; Wang, J.; Li, X. Advancing deep underground research through integration of engineering and science. *Deep Undergr. Sci. Eng.* **2022**, *1*, 1–2. [[CrossRef](#)]
2. Hu, L.; Wang, J.; Karrech, A.; Li, X.; Zhao, P.; Liu, L. Exploring the frontiers of deep underground sciences and Engineer-ing—China Yunlong Lake Laboratory is striving to be the best. *Deep Undergr. Sci. Eng.* **2022**, *1*, 130–136. [[CrossRef](#)]
3. Sousa, R.L.; Einstein, H.H. Lessons from accidents during tunnel construction. *Tunn. Undergr. Space Technol.* **2021**, *113*, 103916. [[CrossRef](#)]
4. Liu, J.; Sun, Y.; Li, C.; Yuan, H.; Chen, W.; Liu, X.; Zhou, X. Field monitoring and numerical analysis of tunnel water inrush and the environmental changes. *Tunn. Undergr. Space Technol.* **2022**, *122*, 104360. [[CrossRef](#)]
5. Li, S.; Gao, C.; Zhou, Z.; Li, L.; Wang, M.; Yuan, Y.; Wang, J. Analysis on the precursor information of water inrush in karst tunnels: A true triaxial model test study. *Rock Mech. Rock Eng.* **2019**, *52*, 373–384. [[CrossRef](#)]
6. Yang, W.; Yang, X.; Fang, Z.; Shi, S.; Wang, H.; Bu, L.; Li, L.; Zhou, Z. Model test for water inrush caused by karst caves filled with confined water in tunnels. *Arab. J. Geosci.* **2019**, *12*, 749. [[CrossRef](#)]
7. Zhou, Y.; Li, S.; Li, L.; Shi, S.; Zhang, Q.; Chen, D.; Song, S. 3D fluid-solid coupled model test on water-inrush in tunnel due to seepage from filled karst conduit. *Chin J Rock Mech Eng* **2015**, *34*, 1739–1749.

8. Wang, Y.; Chen, F.; Li, X.; Yin, X.; Lei, Y. The variable-mass seepage law of broken porous rock: An experimental study. *Geomat. Nat. Hazards Risk* **2020**, *11*, 1991–2005. [[CrossRef](#)]
9. Li, G.; Wang, K.; Gong, B.; Tao, Z.G.; Du, K. A multi-temporal series high-accuracy numerical manifold method for transient thermoelastic fracture problems. *Int. J. Solids Struct.* **2021**, *230–231*, 111151. [[CrossRef](#)]
10. Wang, Y.; Gong, B.; Zhang, Y.; Yang, X.; Tang, C. Progressive fracture behavior and acoustic emission release of CJBs affected by joint distance ratio. *Mathematics* **2022**, *10*, 4149. [[CrossRef](#)]
11. Fu, M.; Zhao, G.F. High-performance computing of 3D blasting wave propagation in underground rock cavern by using 4D-LSM on TianHe-3 prototype E class supercomputer. *Deep Undergr. Sci. Eng.* **2022**, *1*, 87–100. [[CrossRef](#)]
12. Chen, T.T.; Foulger, G.R.; Tang, C.A.; Mathias, S.A.; Gong, B. Numerical investigation on origin and evolution of polygonal cracks on rock surfaces. *Eng. Geol.* **2022**, *311*, 106913. [[CrossRef](#)]
13. Li, S.; Liu, H.; Li, L.; Zhang, Q.; Wang, K.; Wang, K. Large scale three-dimensional seepage analysis model test and numerical simulation research on undersea tunnel. *Appl. Ocean Res.* **2016**, *59*, 510–520. [[CrossRef](#)]
14. Jiang, Y.; Zhou, P.; Zhou, F.; Lin, J.; Li, J.; Lin, M.; Yongli, Q.; Wang, Z. Failure analysis and control measures for tunnel faces in water-rich sandy dolomite formations. *Eng. Fail. Anal.* **2022**, *138*, 106350. [[CrossRef](#)]
15. Fan, H.; Li, L.; Chen, G.; Liu, H.; Gao, J.; Li, C.; Peng, X.; Zhou, S. Analysis method of the water inrush and collapse in jointed rock mass tunnels: A case study. *Eng. Anal. Bound. Elem.* **2023**, *146*, 838–850.
16. Yan, F.; Qiu, W.; Sun, K.; Jiang, S.; Huang, H.; Hong, Y.; Hou, Z. Investigation of a large ground collapse, water inrush and mud outburst, and countermeasures during subway excavation in Qingdao: A case study. *Tunn. Undergr. Space Technol.* **2021**, *117*, 104127. [[CrossRef](#)]
17. Huang, Z.; Zhao, K.; Li, X.; Zhong, W.; Wu, Y. Numerical characterization of groundwater flow and fracture-induced water inrush in tunnels. *Tunn. Undergr. Space Technol.* **2021**, *116*, 104119. [[CrossRef](#)]
18. Kavvadas, M.J. Monitoring ground deformation in tunnelling: Current practice in transportation tunnels. *Eng. Geol.* **2005**, *79*, 93–113. [[CrossRef](#)]
19. Masini, L.; Gaudio, D.; Rampello, S.; Romani, E. Observed Performance of a Deep Excavation in the Historical Center of Rome. *J. Geotech. Geoenvironmental Eng.* **2021**, *147*, 05020015. [[CrossRef](#)]
20. Liu, F.; Zhang, Y.; Ma, T.; Tang, C.A. Observed performance of a deep excavation of Qingdao Metro Line 4 in China. *Tunn. Undergr. Space Technol.* **2022**, *123*, 104445. [[CrossRef](#)]
21. Wang, Y.; Li, J.; Wang, Z.F.; Chang, H. Structural failures and geohazards caused by mountain tunnel construction in fault zone and its treatment measures: A case study in Shaanxi. *Eng. Fail. Anal.* **2022**, *138*, 106386. [[CrossRef](#)]
22. Chen, L.; Wang, Z.; Wang, Y.; Bai, X.; Lai, J. Characteristics and failure analysis of a railway tunnel collapse influenced by cavity in phyllite strata. *Eng. Fail. Anal.* **2022**, *142*, 106794. [[CrossRef](#)]
23. Liu, J.; Li, Z.; Zhang, X.; Weng, X. Analysis of Water and Mud Inrush in Tunnel Fault Fracture Zone—A Case Study of Yonglian Tunnel. *Sustainability* **2021**, *13*, 9585. [[CrossRef](#)]
24. Liu, N.; Pei, J.; Cao, C.; Liu, X.; Huang, Y.; Mei, G. Geological investigation and treatment measures against water inrush hazard in karst tunnels: A case study in Guiyang, southwest China. *Tunn. Undergr. Space Technol.* **2022**, *124*, 104491. [[CrossRef](#)]
25. Cheng, S.; Li, S.; Li, L.; Shi, S.; Zhou, Z.; Wang, J. Study on energy band characteristic of microseismic signals in water inrush channel. *J. Geophys. Eng.* **2018**, *15*, 1826–1834. [[CrossRef](#)]
26. Gong, B.; Liang, Z.Z.; Liu, X.X. Nonlinear deformation and failure characteristics of horseshoe-shaped tunnel under varying principal stress direction. *Arab. J. Geosci.* **2022**, *15*, 475. [[CrossRef](#)]
27. Wang, Y.; Gong, B.; Tang, C. Numerical investigation on anisotropy and shape effect of mechanical properties of columnar jointed basalts containing transverse joints. *Rock Mech. Rock Eng.* **2022**, *55*, 7191–7222. [[CrossRef](#)]
28. Chen, G.; Liu, X.; Song, D. Research on in situ stress inversion of deep-buried tunnel based on pressure/tension axis mechanism and geological structure. *Deep Undergr. Sci. Eng.* **2023**, *2*, 1–13. [[CrossRef](#)]
29. Feng, X.H.; Gong, B.; Cheng, X.F.; Zhang, H.H.; Tang, C.A. Anisotropy and microcrack-induced failure precursor of shales under dynamic splitting. *Geomat. Nat. Hazards Risk* **2022**, *13*, 2864–2889. [[CrossRef](#)]
30. Guillermo Federico, S.L. Stochastic and Economic Evaluation of Adaptability in Tunneling Design and Construction. Ph.D. Dissertation, Massachusetts Institute of Technology, Cambridge, MA, USA, 1983.
31. Nilsen, B.; Palmström, A.; Stille, H. Quality control of a sub-sea tunnel project in complex ground conditions. In Proceedings of the ITA World Tunnel Congress, Oslo, Norway, 31 May–3 June 1999; pp. 137–145.
32. Kampmann, J.; Eskesen, S.D.; Summers, J.W. Risk assessment helps select the contractor for the Copenhagen Metro System. In Proceedings of the World Tunnel Congress 1998, São Paulo, Brazil, 25–30 April 1998; pp. 123–128.
33. Wu, Q.; Liu, Y.; Liu, D.; Zhou, W. Prediction of floor water inrush: The application of GIS-based AHP vulnerable index method to Donghuantuo coal mine, China. *Rock Mech. Rock Eng.* **2011**, *44*, 591–600. [[CrossRef](#)]
34. Chen, C.; Zhang, L.; Tiong, R.L.K. A novel learning cloud Bayesian network for risk measurement. *Appl. Soft Comput.* **2020**, *87*, 105947. [[CrossRef](#)]
35. Sousa, R.L.; Einstein, H.H. Risk analysis during tunnel construction using Bayesian Networks: Porto Metro case study. *Tunn. Undergr. Space Technol.* **2012**, *27*, 86–100. [[CrossRef](#)]
36. Zhou, Z.; Goh, Y.M.; Shi, Q.; Qi, H.; Liu, S. Data-driven determination of collapse accident patterns for the mitigation of safety risks at metro construction sites. *Tunn. Undergr. Space Technol.* **2022**, *127*, 104616. [[CrossRef](#)]

37. Pan, Y.; Zhang, L. Mitigating tunnel-induced damages using deep neural networks. *Autom. Constr.* **2022**, *138*, 104219. [[CrossRef](#)]
38. Wang, Z.; Chen, C. Fuzzy comprehensive Bayesian network-based safety risk assessment for metro construction projects. *Tunn. Undergr. Space Technol.* **2017**, *70*, 330–342. [[CrossRef](#)]
39. Pan, Y.; Zhang, L.; Li, Z.; Ding, L. Improved fuzzy Bayesian network-based risk analysis with interval-valued fuzzy sets and D-S evidence theory. *IEEE Trans. Fuzzy Syst.* **2019**, *28*, 2063–2077. [[CrossRef](#)]
40. Wang, X.; Li, S.; Xu, Z.; Lin, P.; Hu, J.; Wang, W. Analysis of factors influencing floor water inrush in coal mines: A nonlinear fuzzy interval assessment method. *Mine Water Environ.* **2019**, *38*, 81–92. [[CrossRef](#)]
41. Kim, J.; Kim, C.; Kim, G.; Kim, I.; Abbas, Q.; Lee, J. Probabilistic tunnel collapse risk evaluation model using analytical hierarchy process (AHP) and Delphi survey technique. *Tunn. Undergr. Space Technol.* **2022**, *120*, 104262. [[CrossRef](#)]
42. Aalianvari, A.; Katibeh, H.; Sharifzadeh, M. Application of fuzzy Delphi AHP method for the estimation and classification of Ghomrud tunnel from groundwater flow hazard. *Arab. J. Geosci.* **2012**, *5*, 275–284. [[CrossRef](#)]
43. Wang, X.; Li, S.; Xu, Z.; Li, X.; Lin, P.; Lin, C. An interval risk assessment method and management of water inflow and inrush in course of karst tunnel excavation. *Tunn. Undergr. Space Technol.* **2019**, *92*, 103033. [[CrossRef](#)]
44. Xue, Y.; Kong, F.; Li, S.; Qiu, D.; Su, M.; Li, Z.; Zhou, B. Water and mud inrush hazard in underground engineering: Genesis, evolution and prevention. *Tunn. Undergr. Space Technol.* **2021**, *114*, 103987. [[CrossRef](#)]

Disclaimer/Publisher’s Note: The statements, opinions and data contained in all publications are solely those of the individual author(s) and contributor(s) and not of MDPI and/or the editor(s). MDPI and/or the editor(s) disclaim responsibility for any injury to people or property resulting from any ideas, methods, instructions or products referred to in the content.